THE JOURNAL OF BIOLOGICAL CHEMISTRY VOL. 284, NO. 24, pp. 16226–16235, June 12, 2009

Elucidating Conformational Changes in the γ-Aminobutyric Acid Transporter-1*

Received for publication, April 2, 2009 Published, JBC Papers in Press, April 10, 2009, DOI 10.1074/jbc.M109.003137

Anne-Kristine Meinild[‡1], Donald D. F. Loo[§], Soren Skovstrup[¶], Ulrik Gether[‖], and Nanna MacAulay[**]

*From the Departments of [‡]Biology, [¶]Medicinal Chemistry, [‖]Neuroscience and Pharmacology, and **Cellular and Molecular Medicine, University of Copenhagen, 2100 Copenhagen, Denmark and the [§]Department of Physiology, David Geffen School of Medicine, University of California, Los Angeles, California 90095-1751*

The GABA transporter-1 (GAT-1) has three current-generating modes: GABA-coupled current, Li^+-induced leak current, and Na^+-dependent transient currents. We earlier hypothesized that Li^+ is able to substitute for the first Na^+ in the transport cycle and thereby induce a distinct conformation in GAT-1 and that the onset of the Li^+-induced leak current at membrane potentials more negative than −50 mV was due to a voltage-dependent conformational change of the Li^+-bound transporter. In this study, we set out to verify this hypothesis and seek insight into the structural dynamics underlying the leak current, as well as the sodium-dependent transient currents, by applying voltage clamp fluorometry to tetramethylrhodamine 6-maleimide-labeled GAT-1 expressed in *Xenopus laevis* oocytes. MTSET accessibility studies demonstrated the presence of two distinct conformations of GAT-1 in the presence of Na^+ or Li^+. The voltage-dependent fluorescence intensity changes obtained in Li^+ buffer correlated with the Li^+-induced leak currents, *i.e.* both were highly voltage-dependent and only present at hyperpolarized potentials (<−50 mV). The transient currents correlated directly with the voltage-dependent fluorescence data obtained in sodium buffer and the associated conformational changes were distinct from those associated with the Li^+-induced leak current. The inhibitor potency of SKF89976A of the Li^+- *versus* Na^+-bound transporter confirmed the cationic dependence of the conformational occupancy. Our observations suggest that the microdomain situated at the external end of transmembrane I is involved in different conformational changes taking place either during the binding and release of sodium or during the initiation of the Li^+-induced leak current.

γ-Aminobutyric acid (GABA)[2] is the major inhibitory neurotransmitter in the mammalian central nervous system. Continuous GABAergic neurotransmission is efficiently prevented by a GABA re-uptake system that transports GABA back into the synaptic processes via the GABA transporters (GAT). Four isoforms of the mammalian GAT have been found: GAT-1, GAT-2, GAT-3, and BGT-1 (betaine transporter-1) (1). These membrane proteins couple the transport of one GABA molecule to the transport of two Na^+ and one Cl^- (2, 3). Accordingly, the transport process is electrogenic and the transport activity can therefore be monitored by electrophysiological methods. GAT-1 has also been shown to generate: (i) an inwardly rectifying leak current in the presence of Li^+ (and in complete absence of Na^+) when the membrane potential is more negative than −50 mV (4–6) and (ii) a presteady-state transient current in the presence of Na^+ but in the absence of GABA in response to step jumps in membrane voltage (4, 7).

GAT-1 is strictly dependent on external Na^+ to drive the transport of GABA (7) and external GABA does not affect the Li^+-induced leak current (8). Taken together, this suggests that Li^+ *cannot* induce the same conformation in GAT-1 as Na^+ is capable of inducing: namely the conformation that is required for the binding and translocation of GABA. This is in contrast to, *e.g.* the related serotonin transporter and dopamine transporter in which substrate inhibits the Li^+-induced leak current (9, 10) and the Na^+/glucose cotransporter (SGLT1) where Li^+ is able to sustain substrate transport (11). We have in an earlier study shown that Li^+ is able to bind to the first low apparent affinity cation-binding site in the transport cycle (and replace Na^+) but not to the second high apparent affinity cation-binding site (8). This finding was later confirmed by Kanner and co-workers (12), who were able to identify the cation-binding site with which Li^+ interacts and is able to replace Na^+. According to our model, the transporter in the presence of Li^+ is "stalled" in the conformation in which only the first cation-binding site is occupied, in contrast to the presence of Na^+, where both cation-binding sites are occupied.

An unresolved question on the Li^+-induced leak current for GAT-1 is the mechanism of the prominent inward rectification. The electrochemical driving force for Li^+ predicts a Li^+-induced inward current originating at much more positive membrane potentials, but this current is not detected unless the membrane potential is more negative than −50 mV. We previously hypothesized that the Li^+-induced leak mode would commence only at the hyperpolarized membrane potentials due to a voltage-dependent conformational change in the Li^+-bound GABA transporter (8). In the present study, we set out to test this hypothesis by introduction of a fluorescent probe in

* The work was supported by the Danish Health Science Research Council, the Novo Nordisk Foundation, the Carlsberg Foundation, the Lundbeck Foundation, and the John and Birthe Meyer Foundation.

[1] To whom correspondence should be addressed: The August Krogh Bldg., Universitetsparken 13, DK-2100 Copenhagen. Tel.: 45-3532-1651; Fax: 45-3532-1567; E-mail: smeinild@bio.ku.dk.

[2] The abbreviations used are: GABA, γ-aminobutyric acid; G, conductance; GAT-1, the GABA transporter 1; $LeuT_{Aa}$, leucine transporter from *Aquifex aeolicus*; MTSET, methanethiosulfonate ethyltrimethylammonium; NMDG, methyl-D-glucamine; SGLT-1, glucose transporter-1; TM, transmembrane helix; TMR6M, tetramethylrhodamine 6-maleimide; V_h, holding membrane potential; V_m, membrane potential; V_t, test membrane potential; $V_{0.5}$, the membrane potential where there is 50% charge transfer or 50% change in fluorescence; z, the apparent valence of the movable charge; Q_{GAT}, transporter-specific charge movement.

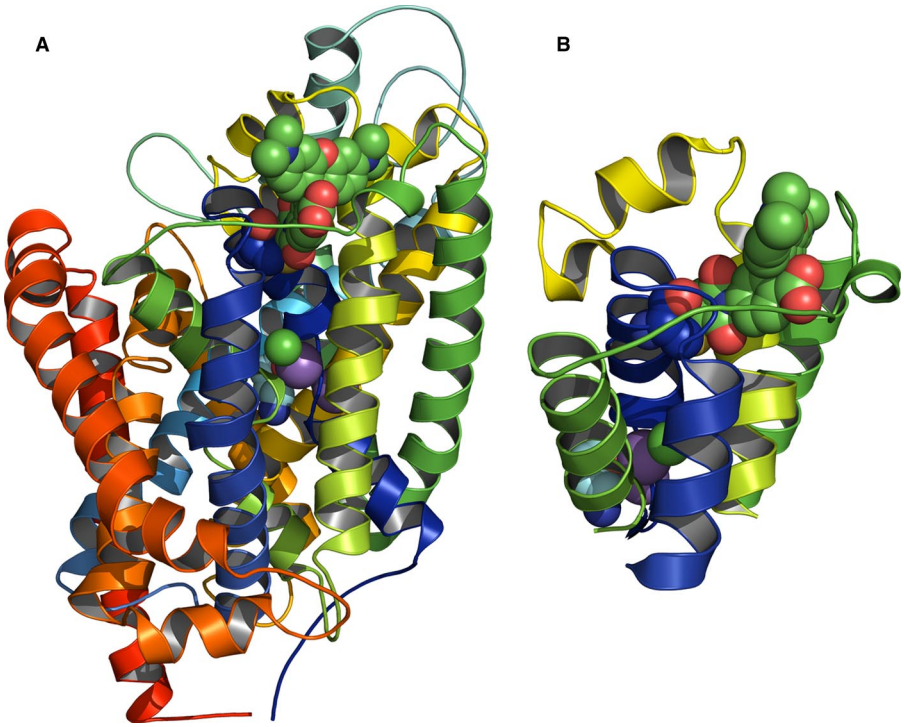

FIGURE 1. **Three-dimensional model of GAT-1 with the fluorophore, TMR6M, covalently attached to Cys^{74}.** The model was made by homology modeling with the bacterial LeuT$_{Aa}$ transporter as template. *A*, side view of the GAT-1 model. The 12 transmembrane helices are shown in different colors; TM1 being *blue* and TM12 being *red*. The two sodium ions are *purple spheres*, chloride is a *green sphere*, and GABA is shown next to the sodium ions as *red*, *light* and *dark blue spheres*. TMR6M is located in the external surface of the model (shown as *green*, *blue*, and *red spheres*) and is attached to Cys^{74} (shown as *blue*, *red*, and *yellow spheres*). *B*, magnified view of the local environment of TMR6M embedded in a hydrophobic cleft between EL3 (*green*), the beginning of EL4 (*yellow*), and the outer part of TM1 (*blue*). Below TMR6M, sodium, chloride, and GABA can be seen as spheres.

GAT-1 to monitor voltage-dependent local conformational changes and relate these to the different current-generating modes of GAT-1.

We expressed GAT-1 in *Xenopus laevis* oocytes and used simultaneous electrical and optical measurements (voltage clamp fluorometry) (13) to monitor the currents and conformational changes of the transporter in the presence of Li^+ and Na^+ in response to step changes in membrane potential. By labeling Cys^{74} at the external end of transmembrane helix (TM) I of rat GAT-1 (see Fig. 1) with the cysteine-reactive fluorescent probe, tetramethylrhodamine 6-maleimide (TMR6M), we were able to correlate the voltage dependence of the Li^+-induced leak current and the Li^+- and voltage-dependent changes in conformations observed by fluorescence intensity changes. The voltage dependence of the Li^+-induced conformational changes appeared distinct from the Na^+-induced conformational changes associated with the Na^+-dependent transient currents. We also explored differences in the inhibitor potency of the GAT-1-specific inhibitor SKF89976A (14) as well as the differential inhibition of the GABA transport by the cysteine-reactive methanethiosulfonate ethyltrimethylammonium (MTSET) in the presence of either Na^+ or Li^+. Finally, we prepared a homology model of GAT-1 (Fig. 1) by using the bacterial leucine transporter, LeuT$_{Aa}$ (15), as a template and dock the TMR6M into the model to provide a framework for interpreting the putative conformational rearrangements that may explain the observed changes in fluorescence intensity.

Altogether, the present data support that local conformational changes taking place at the external surface of TM1 to mirror the global conformational changes taking place during the current-generating modes of the GABA transporter. Moreover, our data demonstrate that voltage dependence of the conformational changes associated with the Li^+-induced leak current is different from the Na^+-dependent conformational changes required for GABA transport.

EXPERIMENTAL PROCEDURES

Molecular Biology and Heterologous Expression in Oocytes—The rat GAT-1 cDNA was in a vector optimized for oocyte expression (pNB1) as earlier described (6). The cDNA was linearized downstream of the poly(A) segment and *in vitro* transcribed with T7 RNA polymerase using the T7 Megascript® kit (Ambion/Applied Biosystems, TX) and 50 ng of cRNA was injected into defoliculated *X. laevis* oocytes. The oocytes were incubated in Kulori medium (90 mM NaCl, 1 mM KCl, 1 mM $CaCl_2$, 1 mM $MgCl_2$, 5 mM HEPES, pH 7.4) at 19 °C for 3–7 days before experiments were performed.

Electrophysiology—The two-electrode voltage clamp method was used to control the membrane potential and monitor the current in oocytes expressing the GAT-1 transporters. Generally, the membrane potential (V_m) of the oocyte was held at −50 mV and the experimental chamber was continuously perfused by a NaCl buffer containing 100 mM NaCl, 2 mM KCl, 1 mM $CaCl_2$, 1 mM $MgCl_2$, 10 mM HEPES, pH 7.4. In the Li^+-induced leak current experiments equimolar Li^+ replaced Na^+ (LiCl buffer) and in Na^+- and Li^+-free experiments, Na^+ was replaced by equimolar methyl-D-glucamine (NMDG) (NMDG-Cl buffer). Two-electrode voltage clamp recordings were performed at room temperature with a Dagan clampator interfaced to an IBM compatible PC using a DigiData 1320 A/D converter and pCLAMP 9.0 (Axon Instruments). Currents were low pass-filtered at 500 Hz and sampled at 2 kHz. Electrodes were pulled from borosilicate glass capillaries to a resistance of 0.5–2 megaohm and were filled with 1 M KCl.

The transporter-specific GABA-coupled current (I_{GABA}) was obtained by subtracting the steady state current in NaCl buffer from the steady state current in NaCl buffer + GABA ($I_{Na+GABA} - I_{Na}$), whereas the Li^+-induced leak current was obtained by subtracting the steady state current in NMDG-Cl buffer from the steady state current in LiCl buffer ($I_{Li} - I_{NMDG}$). For determination of the IC_{50} values for SKF89976A inhibition of the GABA-coupled current, the Li^+-induced leak

current, and the transient currents (see below), the dose-response curves were fitted to the equation: $I_{ss} = I_{max}/(1 + 10^{([SKF8976A]\times logIC_{50})})$, where I_{ss} is the steady-state current, I_{max} is the maximal current, [SKF89976A] is the concentration of the inhibitor, and IC_{50} is the concentration of the inhibitor required to inhibit half the I_{max}.

The transient currents were detected by a pulse protocol where V_m initially was held at −50 mV and then jumped to a series of test potentials (from +50 to −150 mV with 20-mV increments) for 400 ms before returning to V_m. At each test potential, the transporter-specific transient currents were extracted by fitting the relaxation currents to a double exponential decay function: $I_{tot} = I_{mc} \exp(-t/\tau_{mc}) + I_{GAT} \exp(-t/\tau_{GAT}) + I_{ss}$, where I_{tot} is the total current, $I_{mc} \exp(-t/\tau_{mc})$ is the bilayer capacitive current with initial value I_{mc} and time constant τ_{mc}, $I_{GAT} \exp(-t/\tau_{GAT})$ is the GAT-1 transient current with initial value, I_{GAT}, and time constant, τ_{GAT}, I_{ss} is the steady-state current, and t is the time. From such fits, the transporter-specific charge movement, Q_{GAT}, was obtained by integrating the ON or OFF transient currents at different potentials with respect to time. The charge-voltage (Q_{GAT}/V_m) relations were fitted to a Boltzmann function: $(Q - Q_{hyp})/Q_{max} = 1/(1 + \exp(z(V_t - V_{0.5})F/RT))$, where $Q_{max} = Q_{dep} - Q_{hyp}$; Q_{dep} and Q_{hyp} are the Q at depolarizing and hyperpolarizing limits; F is Faradays constant; R, the gas constant; T, the absolute temperature; $V_{0.5}$, the membrane potential where there is 50% charge transfer; and z, the apparent valence of the movable charge (16). For Q_{hyp} to be the hyperpolarizing limit, we assumed z to be negative.

For MTSET experiments, a stock solution (100 mM in water) was prepared fresh on the day of the experiment and stored on ice. Immediately before actual exposure, the stock solution was diluted to a final concentration of 1 mM in either NaCl buffer or LiCl buffer. Exposure of MTSET was done under continuous superfusion, and with the membrane potential clamped to −90 mV. I_{GABA} was determined before and after exposure to MTSET. To estimate the reaction rate constant, k, for MTSET inhibition of I_{GABA} in NaCl or LiCl buffers, we applied MTSET in 2-min intervals and measured the remaining I_{GABA} after each application. The I_{GABA} remaining after each MTSET application as a function of incubation time was then plotted and fitted as described in Ref. 17.

Fluorescence Experiments—For labeling of GAT-1 with the fluorophore, oocytes were incubated for 1½-2 h in NaCl buffer containing 250 μM TMR6M. After labeling, the oocytes were washed thoroughly with NaCl buffer. The three current-generating modes of GAT-1 were affected differently by labeling with TMR6M: the GABA-coupled current was inhibited approximately 75%, whereas the Li^+-induced leak current was affected at membrane potentials more negative than −110 mV, where it was reduced by ~25%. Analysis of the transient currents showed a reduction in the Q_{max} upon labeling with TRM6M, but also a shift in the $V_{0.5}$: GAT-1, $V_{0.5} = -8 \pm 1$ mV and $Q_{max} = 27.8 \pm 0.3$ nC ($n = 3$); TMR6M-labeled GAT-1, $V_{0.5} = 18.3 \pm 15.6$ mV and $Q_{max} = 19.7 \pm 2.0$ nC ($n = 4$). Furthermore, the time constants for the current relaxations were slower after labeling with TMR6M; hence τ_{max} before labeling was 88.5 ± 2.2 ms ($n = 3$) and $\tau_{max} = 112.1 \pm 11.5$ ms ($n = 3$) after labeling with TMR6M (*data not shown*). In the experiments correlating currents directly to the fluorescence signal, we have used GAT-1 labeled with TMR6M, whereas in the experiments examining the inhibitory effect of SKF89976A we have used unlabeled GAT-1.

The combined electrophysiological and fluorescence experiments were performed as described previously (18). In brief, the membrane potential was controlled and currents were measured using the two-electrode voltage clamp as described above. Fluorescence intensity changes were measured using a Hamamatsu S5590 silicon photodiode (Hamamatsu City, Japan) connected to the camera port of an Olympus BX50WI epifluorescence microscope (Olympus America Inc., Melville, NY). The oocyte membrane was illuminated with a 100 W halogen lamp (Olympus) via excitation and emission filters at 535 and 580 nm (Olympus filter set U-M576). An electronic shutter (Uniblitz VS25S2T1, Vincent Associates, Rochester, NY), synchronized with the electrophysiological measurements, was placed between the lamp and the preparation to minimize photobleaching. The experiments were controlled using the program pClamp9 (Axon Instruments, Union City, CA). The transient currents and the fluorescence signal were measured simultaneously. The fluorescent signal was amplified between 20 and 100 times, low-pass filtered at 1 kHz using an eight-pole Bessel filter (LPF-8, Warner Instrument Corp., Hamden, CT), and digitized at 2 kHz. Fluorescence intensity is expressed as arbitrary units.

The fluorescence traces were obtained by holding the membrane potential at −50 mV followed by 500-ms jumps to different test potentials with 20-mV increments, doing 3 runs. The specific test potentials are given in the figure legends. After collecting the data the individual files were corrected for photobleaching (18).

The difference in steady-state fluorescence between the test and holding potentials (ΔF) was obtained by fitting the fluorescence trace at each voltage to a single exponential function. The dependence of ΔF on membrane voltage was obtained by fitting the $\Delta F/V_m$ to a Boltzmann function: $(\Delta F - \Delta F_{hyp})/\Delta F_{max} = 1/[1 + \exp(z(V_m - V_{0.5})F/RT)]$, where $\Delta F_{max} = \Delta F_{dep} - \Delta F_{hyp}$, ΔF_{dep} and ΔF_{hyp} are the ΔF at depolarizing and hyperpolarizing limits, F, R, and T has the same meaning as above, $V_{0.5}$ is the membrane potential at 50% ΔF_{max}, and z is the apparent valence of the charge sensor of the fluorophore.

Homology Modeling of GAT-1—A homology model of the human GABA transporter subtype 1, hGAT-1, was prepared following the alignment of Beuming *et al.* (19) using the bacterial leucine transporter, $LeuT_{Aa}$, as a template. The model was generated using MODELLER 9 version 4 (20). From a set of 150 generated models obtained through the automodel class one structure was picked out and subjected to additional loop refinements via the loop model class as implemented in MODELLER. Model evaluation was done based on the DOPE-score using MODELLERS DOPE assessment method, via the SAVES server, which is a model evaluation server, as well as via visual evaluation of structural motifs.

GABA was docked into the generated GAT-1 model following the Induced Fit Docking protocol as implemented in Schrödingers Maestro program package (21). Conformations of

TMR6M were sampled by a Monte Carlo conformational search, and several conformations were manually attached to Cys^{74}. The manually prepared poses (TMR6M and residues within 6 Å) were subjected to a Prime minimization, and TMR6M was finally redocked into the model by the Prime Covalent Docking script available through Maestro, which yielded only one conformation of TMR6M. Figures were prepared with PyMOL 1.1 (22).

Calculations—The data were analyzed by nonlinear regression analysis using Prism 4.0 (GraphPad Software, San Diego, CA), Clampfit 9.0 (Axon Instruments Inc., Union City, CA), and SigmaPlot (version 8.0, SPSS Inc., Chicago, IL). All numbers are given as mean ± S.E., where values have been obtained from the individual experiments before normalization and with *n* equal to the number of oocytes tested. For most experiments oocytes were obtained from different donor frogs.

RESULTS

MTSET Accessibility to Cys^{74} Is Dependent on the Conformational State of GAT-1—Because our model predicts that the conformational state occupied by the GABA transporter depends on the cation present in the test solution, we exposed oocytes expressing GAT-1 to the membrane-impermeable MTSET to monitor the accessibility to Cys^{74} in the presence of either Li^+ or Na^+. It has previously been shown that transport of GABA is partially blocked by treatment with MTSET dissolved in NaCl buffer (23), hence we determined the magnitude of the GABA-induced current (100 μM GABA in NaCl buffer) before and after incubation in either NaCl buffer or LiCl buffer containing 1 mM MTSET for 6 min and with the membrane potential clamped to −90 mV. The decrease in I_{GABA} was dependent on the cationic composition of the incubation buffer; in NaCl buffer I_{GABA} was decreased to 52 ± 2% ($n = 5$) compared with 29 ± 3% ($n = 5$) after incubation in LiCl buffer ($p < 0.0001$) (Fig. 2*A*). We also determined the reaction rates of MTSET in NaCl buffer compared with LiCl buffer by determination of the progressive decrease in I_{GABA} with increasing cumulative MTSET exposures of 2 min (Fig. 2*B*). We found the reaction rate constant (k) to be almost 2 times higher in LiCl buffer ($k_{Li} = 3.0 \pm 0.6$ min, $n = 4$) compared with NaCl buffer ($k_{Na} = 5.2 \pm 0.4$ min, $n = 4$) ($p = 0.0269$). Thus accessibility to Cys^{74} was increased when Li^+ was bound to GAT-1, indicating that Li^+ induces a unique conformation in GAT-1. The inhibition of I_{GABA} by MTSET is consistent with previous studies on the effect of the membrane-permeable MTSEA on [^{3}H]GABA uptake in cells expressing GAT-1 (24).

Voltage-dependent Fluorescence Changes in TMR6M-labeled GAT-1 Depend on the External Solution—We wished to explore the cationic-specific differences in the voltage-dependent conformational changes by applying the voltage clamp fluorometry method. GAT-1 was expressed in *Xenopus* oocytes and labeled at position Cys^{74} with TMR6M after which changes in fluorescence intensity in response to a series of voltage pulses were monitored. We detected voltage-dependent fluorescence intensity changes (ΔF) with a ratio between the ΔF and the total fluorescence (F), $\Delta F/F$, of 1.1 ± 0.7% ($n = 9$) (ranging from 0.3 to 2.4%) in the NaCl buffer. The time courses of the changes in fluorescence intensity (from −50 mV to the voltages indicated in the each panel) are shown in Fig. 3, *A–C*. These voltage-dependent changes in fluorescence intensity of TMR6M-labeled GAT-1 were highly dependent on the external solution bathing the oocyte. In the NaCl buffer we observed an increase in the fluorescence intensity at membrane potentials more positive than −50 mV, whereas almost no change in the fluorescence intensity was observed upon jumping to membrane potentials more negative than −50 mV (Fig. 3*A*). Bathing the same oocyte in the LiCl buffer showed voltage-dependent changes in fluorescence intensity that were very different. Depolarization of the membrane potential from a holding potential of −50 mV showed only a small increase in the fluorescence signal, whereas hyperpolarization led to a substantial and voltage-dependent decrease in the fluorescence signal (Fig. 3*B*). In the absence of both Na^+ and Li^+ (in NMDG-Cl buffer), voltage-dependent changes in the fluorescence signal were also observed. These changes were symmetrical around the holding potential and

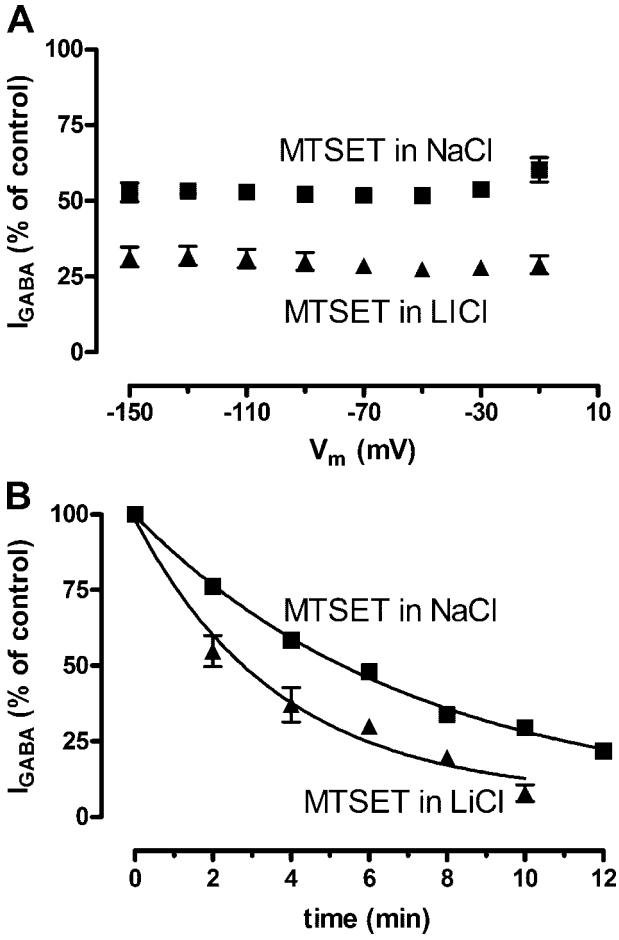

FIGURE 2. **Effect on the GABA-coupled current in GAT-1 expressing oocytes upon incubation with 1 mM MTSET in NaCl buffer and LiCl buffer.** *A*, I_{GABA} plotted as function of membrane potential after incubation with 1 mM MTSET in either NaCl buffer (*squares*) or LiCl buffer (*triangles*) for 6 min with the membrane potential held at −90 mV. After incubation in NaCl buffer, I_{GABA} was inhibited to 52 ± 2% ($n = 5$) and after incubation in LiCl buffer to 29 ± 3% ($n = 5$). The degree of inhibition was independent of the membrane potential. *B*, I_{GABA} plotted as a function of time after cumulative incubations with MTSET in either NaCl buffer (*squares*) or LiCl buffer (*triangles*) for 2-min periods with the membrane potential held at −90 mV. The *lines* represent the fits for obtaining the reaction rate constant, k, MTSET incubation in NaCl buffer gave a k_{Na} of 5.2 ± 0.4 min ($n = 4$) and MTSET incubation in LiCl buffer gave a k_{Li} of 3.0 ± 0.6 min ($n = 4$).

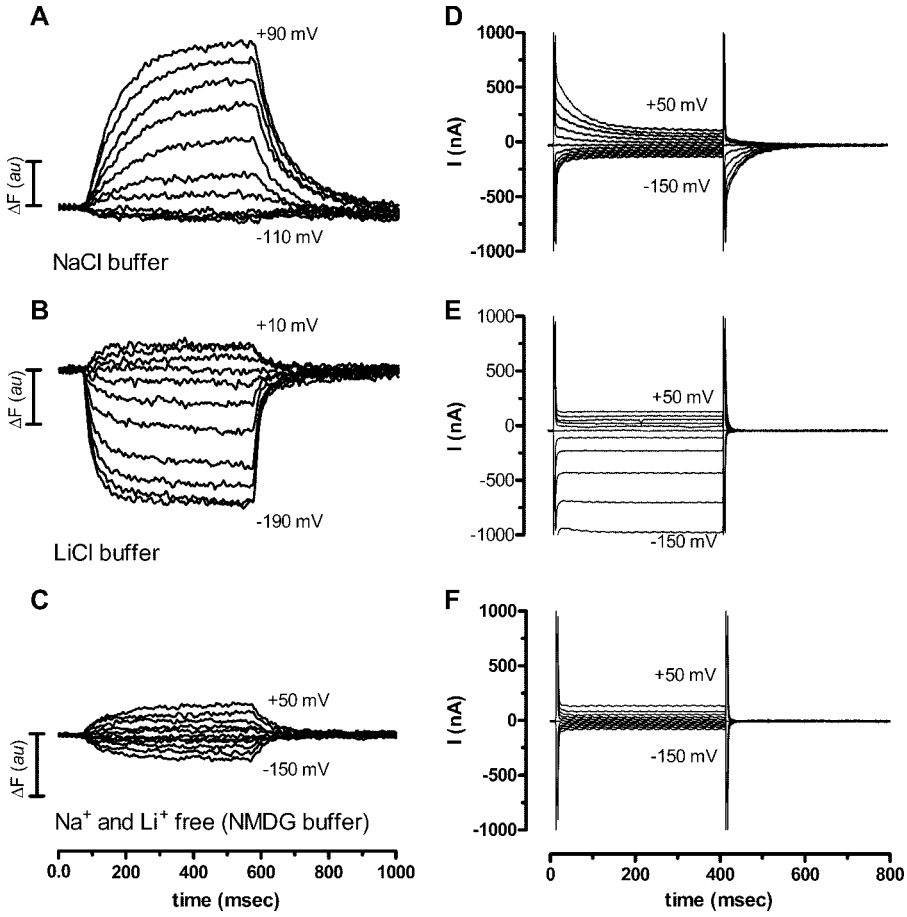

FIGURE 3. **Fluorescence intensity changes and total current records obtained in voltage jump experiments on TMR6M-labeled GAT-1-expressing oocytes.** *A–C*, time course of the voltage-dependent fluorescence signal intensity measured in different external solutions. *A*, experiment performed in NaCl buffer with the membrane potential (V_m) held at −50 mV (V_h) and then stepped to test potentials (V_t) from +90 to −110 mV in 20-mV increments for 500 ms before returning to V_h. *B*, experiment performed in LiCl buffer from a V_h of −50 mV to V_t values ranging from +10 mM to −190 mV, otherwise as described above. *C*, experiment performed in NMDG-Cl buffer from a V_h of −50 mV and V_t values from +50 to −150 mV. All three measurements were obtained in the same oocyte and are representative for $n = 5$. *D-F*, total current records from an oocyte expressing GAT-1 and labeled with TMR6M measured in different external solutions with a V_h of −50 mV and subsequent stepping to the V_t value from +50 to −150 mV with 20-mV increments for 400 ms before returning to V_h. *D*, NaCl buffer. *E*, LiCl buffer. *F*, absence of Na^+ and Li^+ (NMDG-Cl buffer). All three measurements were obtained in the same oocyte and are representative for $n = 4$. *au*, arbitray unit.

smaller than those observed in both NaCl and LiCl buffer (Fig. 3*C*). When bathed in NaCl buffer containing 1 mM GABA we observed only very small voltage-dependent fluorescence changes (10 times lower than in NaCl buffer) in the voltage range applied in these experiments ($\Delta F/F < 0.1\%$, $n = 2$) (data not shown). In the GAT-1 C74A mutant, where Cys^{74} has been mutated to a non-reactive alanine, $\Delta F/F$ was <0.05% ($n = 2$).

Voltage-dependent Fluorescence Changes Correlate with Electrophysiological Data—Total current records obtained by voltage jump experiments on GAT-1-expressing oocytes labeled with TMR6M are shown in Fig. 3, *D–F*. There was a clear correlation (see below) between the voltage-dependent fluorescence changes and transient current data obtained in NaCl buffer (Fig. 3, *A* and *D*) and between the voltage-dependent fluorescence changes and the steady-state Li^+-induced leak currents obtained in LiCl buffer (Fig. 3, *B* and *E*). On the contrary, there were no detectable transporter-associated transient or steady-state currents to correlate to the fluorescence changes obtained in NMDG-Cl buffer (Fig. 3, *C* and *F*).

The relative change in fluorescence signal intensity (ΔF), obtained by fitting the Na^+ and voltage-dependent fluorescence changes at each test potential to a single exponential equation, and the Na^+-dependent transporter-specific charge movements (Q_{GAT}) (see "Experimental Procedures") were normalized and plotted as a function of the membrane potential (Fig. 4*A*). The data were fitted to the Boltzmann function to derive the $V_{0.5}$ value for ΔF and Q_{GAT}: ΔF_{Na} $V_{0.5}$ was 9.5 ± 2.4 mV ($n = 9$) and the Q_{GAT} $V_{0.5}$ was 18.8 ± 7.3 mV ($n = 4$). Within the experimental error these two $V_{0.5}$ values are identical to each other ($p = 0.14$). Fig. 4*B* shows the time constants obtained from fitting the fluorescence signals and the charge movements to the exponential equations described above. These time constants coincide, which indicates a close relationship between the fluorescence signals and the charge movements.

Fig. 3*E* shows a voltage jump experiment performed in LiCl buffer with GAT-1 labeled with TMR6M. As previously reported, this Li^+-induced leak current is inwardly rectifying and initiates at a membrane potential more negative than −50 mV. It was not possible to detect any presteady-state transient currents in the LiCl buffer; either these were not present or faster than the time resolution of the current measurements. However, under the assumption that the Li^+ conductance (obtained from the relationship: $I_{Li} = G_{Li}$ ($V_h - V_{eq}(Li)$), where G_{Li} is the Li^+ conductance, V_h is the holding membrane potential, and $V_{eq}(Li)$ is the equilibrium potential for lithium ($[Li]_{in} = 0.001$ mM) is a monitor for protein conformation, the normalized Li^+ conductance plotted as function of the membrane potential was compared with the normalized ΔF_{Li} plotted as a function of the membrane potential as seen in Fig. 4*A*. At membrane potentials more negative than −150 mV the Li^+ conductance begins to saturate (see Fig. 4*A*), and hence it was possible to determine a $V_{0.5}$ for both the G_{Li} (−125 ± 4.2 mV, $n = 5$) and ΔF_{Li} (−101.7 ± 2.8 mV, $n = 9$) by fitting the data to the Boltzmann function. These two values are numerically close although still significantly different ($p = 0.0005$); however, both are significantly different from those of the Na^+-dependent conformational changes ($p = 0.0001$). In Fig. 4*B*, the time constants of the ΔF_{Li} are plotted as function of the membrane potential. These were faster and less dependent on the membrane voltage as compared with the time constants

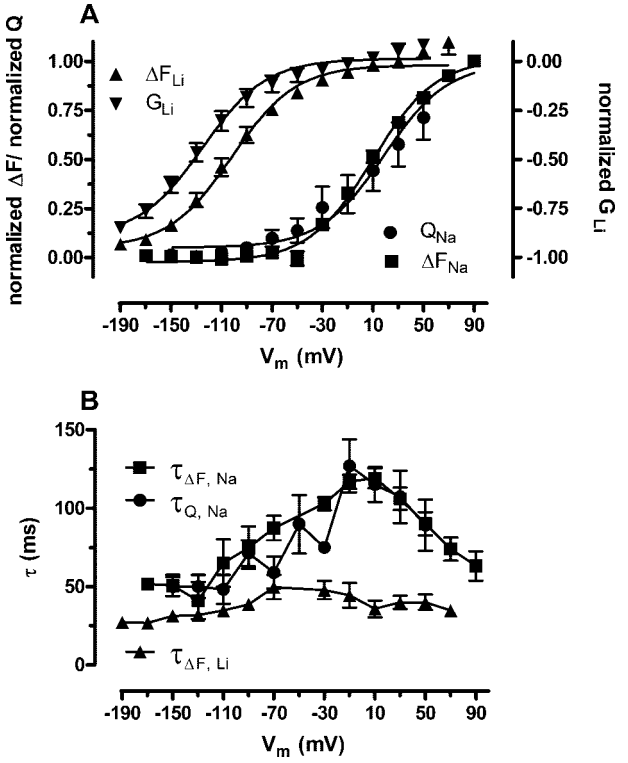

FIGURE 4. **The voltage-dependent fluorescence changes correlate well with the current-generating modes of TMR6M-labeled GAT-1.** *A*, normalized $\Delta F/V_m$ relationship for the fluorescence signal in NaCl buffer (ΔF_{Na}, *squares*) was fitted to a Boltzmann function (*solid lines*). The $V_{0.5}$ obtained from the fit was 9.5 ± 2.4 mV ($n = 9$). The Q_{GAT}-V_m relationship for the Na^+-dependent transient currents were normalized, plotted (Q_{GAT}, *circles*), and fitted to the Boltzmann equation (*solid line*) giving a $V_{0.5}$ of 18.8 ± 7.3 mV ($n = 4$). Normalized ΔF-V_m relationship for the fluorescence signal in LiCl buffer (ΔF_{Li}, *up triangles*) was fitted to a Boltzmann function (*solid line*). The $V_{0.5}$ obtained for the fit was −101.7 ± 2.8 mV ($n = 9$). Normalized g-V_m relationship for the Li^+ conductance (G_{Li}, *down triangles*) was also fitted (*solid line*) to obtain a $V_{0.5}$ of −125 ± 4.2 ($n = 5$). *B*, the τ/V_m relationship for the ΔF in NaCl ($\tau_{\Delta F,Na}$, *squares*) and LiCl buffers ($\tau_{\Delta F,Li}$, *up triangles*), and for transient currents in NaCl ($\tau_{Q,Na}$, *circles*). In NaCl buffer, ΔF_{Na} τ_{max} = 19.1 ± 6.3 ms ($n = 10$) at a V_m of +10 mV and Q_{GAT} τ_{max} = 112.1 ± 11.5 ms ($n = 5$) at a V_m of −10 mV. The time constants for both Q_{GAT} and ΔF_{Na} depend on the membrane potential and varied between 50.6 ± 6.9 (at −150 mV) and 119.1 ± 6.3 ms (at +10 mV) ($n = 10$). In LiCl buffer the ΔF_{Li} τ_{max} = 49.7 ± 7.9 ms ($n = 9$) at a V_m of −70 mV. The time constants for ΔF_{Li} throughout the tested membrane potentials ranged from 27.3 ± 2.8 to 49.7 ± 7.9 ($n = 9$).

obtained for the Na^+-dependent Q_{GAT} and ΔF_{Na}. To obtain information about the time course of the Li-induced leak current *per se*, we subtracted the current traces obtained in NMDG-Cl buffer from those obtained in LiCl buffer, and fitted the resulting current trace specific for the Li^+-induced leak to a single exponential decay function. The time constants obtained from these fits indicated that full activation of the Li^+-induced leak current was achieved within 4 ms (data not shown). This is an order of magnitude faster than the time constants observed for the fluorescence intensity changes in LiCl buffer.

We also analyzed the voltage dependence of the ΔF_{NMDG} and the corresponding time constants in NMDG-Cl buffer. There was no saturation of the voltage-dependent ΔF_{NMDG} within the range tested (from +50 to −150 mV); and the time constants were independent of the membrane potential with an average τ_{NMDG} of 76 ± 13 ms ($n = 3$) (data not shown). The fluorescence intensity changes in NMDG-Cl buffer indicates that voltage-dependent conformational changes take place even in the absence of a monovalent cation. These conformational changes are believed to represent the conformational transition of the empty transporter between inward-facing and outward-facing conformations with a very small (if any) accompanying charge movement (25).

Inhibition by the Specific Inhibitor SKF89976A: Voltage-dependent Fluorescence Changes—To confirm that the voltage-dependent fluorescence intensity changes were directly associated with GAT-1, we employed the specific inhibitor, SKF89976A (14). In the initial experiments, the voltage-dependent fluorescence intensity changes were detected in the absence and presence of 50 μM SKF89976A, a concentration well above the $IC_{50(SKF89976A)}$ for the GABA-coupled current (see below). Fig. 5, *A* and *B*, show the fluorescence traces obtained in NaCl buffer ± SKF89976A, where 50 μM SKF89976A blocked the ΔF_{Na} signals, verifying that the ΔF_{Na} signals are indeed specific for GAT-1. Fig. 5, *C* and *D*, shows the fluorescence traces obtained in the LiCl buffer ± 50 μM SKF89976A. In this external solution the given concentration of inhibitor only partially blocked the ΔF_{Li} signals, indicating that the Li^+-bound conformation of GAT-1 interacted differently with SKF89976A. To test if it was possible to completely block the voltage-dependent changes in fluorescence intensity in the presence of Li^+, the experiments were carried out with increasing concentrations of SKF89976A. The fluorescence signal was completely blocked in the presence of 2 mM SKF89976A in the LiCl buffer (data not shown). This difference in potency of SKF89976A inhibition of the fluorescence signal in NaCl buffer and LiCl buffer indicates that the Li^+-bound GAT-1 may occupy a conformation that is distinct from the Na^+-bound GAT-1.

Inhibition by the Specific Inhibitor SKF89976A: Three Current-generating Modes of GAT-1—Also with respect to electrophysiological experiments, SKF89976A showed different inhibitory effects on the three current-generating modes of GAT-1, that we have investigated in this study (Fig. 6). We determined the IC_{50} for SKF89976A inhibition of the GABA-coupled current at saturating GABA concentrations (100 μM) and found an IC_{50} value of 4.3 ± 1.1 μM ($n = 5$) at −70 mV, which was independent of the membrane potential. For the Li^+-induced leak current, the IC_{50} value was dependent on the membrane potential: at −110 mV the IC_{50} was at its highest value, 218 ± 28 μM ($n = 6$), declining toward lower values at membrane potentials more or less hyperpolarized (for example, IC_{50} was 152 ± 23 μM ($n = 6$) and 105 ± 22 μM ($n = 6$) at −150 and −70 mV, respectively). For inhibition of the transporter-specific transient current, the IC_{50} determined from the decrease in Q_{max} was 0.24 ± 0.11 μM ($n = 3$).

DISCUSSION

We have in the present paper employed voltage clamp fluorometry to investigate the conformational changes associated with the Li^+-induced leak mode and the Na^+-dependent transient currents in the rat GABA transporter-1. The voltage-dependent fluorescence changes of the TRM6M-labeled Cys^{74} in the external end of TM1 mirrored the global conformational changes that give rise to the Li^+-induced leak currents as well as the Na^+-dependent transient currents. We have shown here

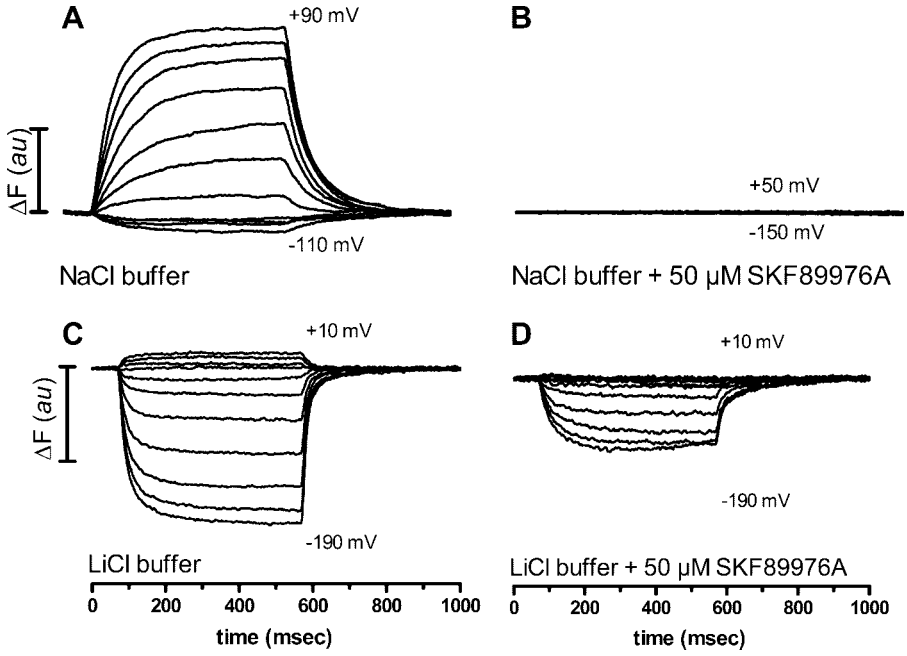

FIGURE 5. **SKF89976A show different inhibition degrees of the voltage-dependent fluorescence intensity changes depending on the external solution.** *A* and *B*, addition of 50 μM SKF89976A to the NaCl buffer completely blocked the voltage-dependent changes of the fluorescence signal, compare *panels A* and *B*. *C* and *D*, addition of 50 μM SKF89976A to the LiCl buffer abolished the voltage-dependent changes in the fluorescence signal at depolarizing potentials, whereas there was only a partial decrease in the fluorescence signal at hyperpolarizing potentials; compare *panels C* and *D*. *au*, arbitrary unit.

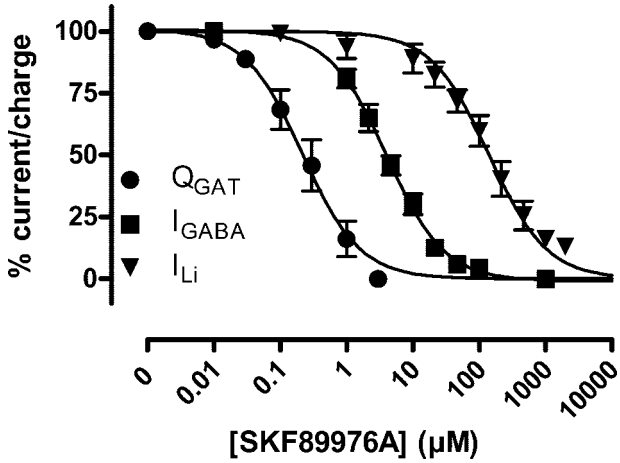

FIGURE 6. **Inhibition of the GABA-coupled current, the Li^+-induced leak current, and the Na^+-dependent transient current with SKF89976A.** *A*, normalized dose-response curves for the GABA-coupled currents at −70 mV (I_{GABA}, *squares*), the Li^+-induced leak current at −150 mV (I_{Li}, *down triangles*), and the Q_{max} values obtained from transient current data (Q_{GAT}, *circles*) plotted as function of the SKF89976A concentration. These relationships were fitted to give the following $IC_{50(SKF89976A)}$ values for I_{GABA}, 4.3 ± 1.0 μM ($n = 5$); for I_{Li}, 152 ± 23 μM ($n = 6$); and for the transient currents, 0.24 ± 0.11 μM ($n = 3$).

that the time course and voltage dependence of the Li^+-induced conformational changes are indeed distinct from those of the Na^+-induced conformational changes.

Cys^{74} is located at the external end of TM1, which is one of the transmembrane domains that are proposed to play a key role in the conformational changes associated with coordination of the first cation (Na2 in $LeuT_{Aa}$) and Na^+/substrate transport according to a model derived from the crystal structure of the bacterial homologue $LeuT_{Aa}$ (15, 26). Mutational studies of residues in TM1 prior to the publication of the crystal structure and sequence alignment of GAT-1 to $LeuT_{Aa}$ have identified amino acids in TM1 that are involved in Na^+ binding (the high-affinity Na^+-binding site), interactions with the substrate, as well as conformational transitions (4, 12, 27–32). Our observations of the close relationship between current (global conformational changes and overall function) and fluorescence (local conformational changes) are consistent with this hypothesis.

The Li^+-induced Leak Current—The GAT-1 as well as related transport proteins such as serotonin transporter, dopamine transporter, and the noradrenalin transporter from the SLC6 family as well as the more distantly related SGLT1 from the SLC5 family have been shown to support cationic uncoupled leak currents in the absence of substrate (4–6, 9, 10, 33, 34). The GAT-1 is unique among this group as it does *not* conduct Na^+-induced leak currents; but rather supports an inwardly rectifying Li^+-induced leak current (4–6), which has been shown to be inhibited by millimolar Na^+ concentrations (8, 28) in a non-competitive manner (28). Based on these findings, we have earlier proposed a model in which Li^+ is able to bind to the first "low apparent affinity" cation-binding site and thereby partly substitute for Na^+ in the transport cycle (8). Asp^{395} was recently shown to be the coordinating residue for the Li^+ interaction at this first cation-binding site and mutation of this residue abolished the Li^+-induced leak current as well as the stimulating effect of Li^+ on the Na^+-dependent GABA transport (12). Li^+ is, however, not able to substitute for Na^+ in the second "high apparent affinity" cation-binding site and therefore GABA transport does not take place in a Li^+ buffer (7, 8). It follows that binding of the second cation (Na^+) drives the transporter into a conformation in which GABA is able to bind and in which there is no leak current.

In our model (Fig. 7), this is depicted as the C_1 state with one Na^+ or one Li^+ bound to the first cation-binding site being different from the C_2 state, which is occupied by two Na^+. We hypothesize that the conformation of the transporter would be similar when only one cation was bound at the first cation-binding site (independent on whether it was Na^+ or Li^+), although we have no experimental evidence to base this on. Li^+ has been suggested to introduce a distinct conformation in GAT-1 based on the transporter-specific different passive water permeabilities in the presence of Li^+ or Na^+ (8) and the different level of MTSEA inhibition of GAT-1 (24). Li^+ has likewise been shown to induce the formation of a distinct conformation in the related serotonin transporter (35, 36) and in

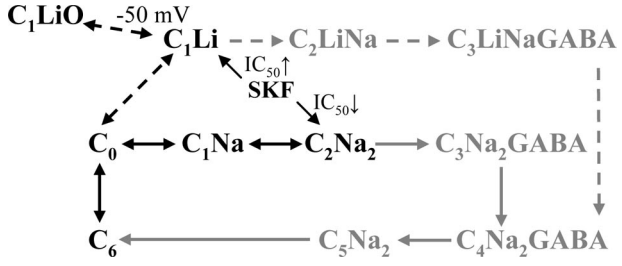

FIGURE 7. **Illustration of GAT-1 transport model (modified from Ref. 8).** The C_6 and C_0 states represent the empty transporters with the binding sites facing the intracellular and extracellular sites, respectively. In NaCl buffer, the transporter binds the two ions sequentially, states C_1Na and C_2Na_2. The Na^+-dependent transient currents are thought to be due to the partial reactions: $C_6 \leftrightarrow C_0 \leftrightarrow C_1Na \leftrightarrow C_2Na_2$. In LiCl buffer, the transporter binds one lithium ion (C_1Li) and membrane potentials more negative than −50 mV lead to opening of the conducting mode of the protein (C_1LiO). SKF89976A binding to the protein is described by the IC_{50} values: in C_1Li (for the leak current), the SKF89976A IC_{50} is higher than for the inhibition of the GABA-coupled current, whereas in C_2Na_2 (for the transient currents) the IC_{50} is lower, as indicated by the *arrows*. The *gray* illustrations show the GABA transport modes of the transporter are not dealt with in this study and the Cl^- is omitted for clarity.

the glycine transporter (37). The presence of a distinct Li^+-bound conformation of GAT-1 was further verified in the present work by the different MTSET accessibilities to Cys^{74} in the presence of either Li^+ or Na^+, although a putative difference in their K_D values and the effect on the MTSET accessibility cannot be ruled out.

The Li^+-induced leak current is strongly rectifying; the current does not commence until the membrane potential of the GAT-1 expressing oocyte has been hyperpolarized to a value more negative than −50 mV, although the electrochemical potential for Li^+ would dictate an inward current arising at a much more positive potential. We previously hypothesized that the Li^+-occupied transporter in the face of a hyperpolarized potential (more negative than −50 mV) would change into a "leaky" conformation, in which the transporter acts as a channel (8). To verify this hypothesis experimentally we employed the voltage clamp fluorometry method in the present study. By labeling Cys^{74} of the GAT-1-expressing oocytes with a fluorescent dye, TRM6M, we have shown that the Li^+-bound transporter undergoes voltage-dependent conformational changes that reflect the voltage dependence of the Li^+-induced leak current. We therefore propose that the leak state arises at membrane potentials more negative than −50 mV due to a voltage-dependent conformational change from a Li^+-bound "tight" conformation to a leaky conformation (Fig. 7, $C_1Li \leftrightarrow C_1LiO$). This conformational change occurs in two steps: a very quick voltage-dependent opening of the Li^+ conductance pathway followed by a slower conformational change (monitored by fluorescence with a time constant of 25–50 ms, Fig. 4*B*). The parameters describing these two processes are not identical as revealed by the small displacement of the $V_{0.5}$ values for G_{Li} and ΔF_{Li} (seen in Fig. 4*A*).

Earlier findings of a Li^+-induced increase in open probability of single-channel activity in the related serotonin transporter (38), the lack of water co-transport in the Li^+-induced leak mode of GAT-1 (8), taken together with saturation of the voltage-dependent fluorescence changes associated with the conversion from one conformation to another (as opposed to a continuous transport cycle mode) points to the Li^+-induced leak current as a channel mode of operation. The lack of a Na^+-induced leak current in the GABA transporter is, according to the model, explained by the specificity and high apparent Na^+ affinity of the second cation-binding site: with Na^+ present (even a few millimolar), the transporter will primarily occupy the C_2 state, in which the transporter does not exhibit leakage (Fig. 7). As mentioned above, the lack of a Na^+-induced leak current is specific to GAT-1 as related transporters, such as serotonin transporter (9), dopamine transporter (10), SGLT (11, 33), and noradrenalin transporter (34) support a Na^+- as well as a Li^+-induced leak current.

Na^+-dependent Transient Currents and Conformational Changes—The GAT-1 as well as other cotransport proteins such as SGLT1 (25) and the glutamate transporter, EAAT2 (39), display Na^+-dependent transient currents upon step jumps in membrane potential (4, 7). These capacitive transient currents are thought to reflect the transport protein altering its conformational equilibrium between the inward-facing empty transporter (C_6), the outward facing empty transporter (C_0), and the Na^+-bound transporter (C_1 and C_2) (4, 16). As we are not able to resolve the individual steps, the resulting time constants could reflect any of the three transitions or a combination thereof. In the present study we have shown that the Na^+-dependent fluorescence changes upon voltage jumps reflect the voltage dependence and the time constant of the Na^+-dependent transient currents. Thus the *local* conformational changes at the external surface of TM1 follow a similar time course and voltage sensitivity of the conformational changes associated with the transient currents.

In addition, we have shown that the conformational changes (detected by changes in fluorescence intensity) in the absence of cations such as Na^+ and Li^+ can be driven by voltage. The accompanying charge movement is very small or very fast, if any, and beyond the resolution of the current measurements. We assign these conformational changes to the empty transporter alternating between the inward-facing C_6 and the outward-facing C_0 (16, 40). But given the large voltage-dependent fluorescence intensity changes in the presence of Na^+ and Li^+ as compared with NMDG, the local environment of the fluorophore experiences the largest changes in the steps involving cation interaction. The time constant of the fluorescence change in NMDG-Cl buffer was around 80 ms and independent of membrane potential. This is compatible with the overall transport rate, estimated to be 5–10 s^{-1} (4, 41). Nevertheless, this distinct $C_6 \leftrightarrow C_0$ transition rate might very well be highly dependent on the concentration of extracellular Na^+ (as the apparent Na^+ affinity of the first cation binding site is highly voltage dependent (42)) and therefore be much faster during GABA-transport.

Inhibition by SKF89976A—If GAT-1 does indeed occupy two distinct conformations in the presence of Na^+ and Li^+, one could speculate that the GAT-1-specific inhibitor SKF89976A would interact differently with those conformations, resulting in different IC_{50} values. It has previously been shown for the serotonin transporter that replacing external Na^+ with Li^+ induced a distinct conformation as well as a change in K_D for cocaine (36). The GAT-1-specific inhibitor SKF89976A has been shown to completely inhibit the GABA-coupled current

as well as the transient currents in the micromolar range (7), whereas the Li^+-induced leak current, however, was only partially inhibited by this inhibitor concentration (6). The same inhibitory pattern was also observed for the voltage-dependent fluorescence in the present study. The Na^+-dependent fluorescence changes were completely abolished in the presence of 50 μM SKF89976A, whereas the Li^+-dependent fluorescence changes were only partly abolished by the same inhibitor concentration. With an increase in the SKF89976A concentration to the millimolar range, the voltage-dependent fluorescence changes in Li^+ were completely abolished, suggesting a higher $IC_{50(SKF89976A)}$ for the Li^+-bound conformation. We obtained the IC_{50} for the Na^+-dependent transient currents (0.2 μM), the GABA-coupled currents (4 μM), and the Li^+-induced leak currents (100 to 220 μM, voltage-dependent). From these IC_{50} values, we see that the different transport modes display different sensitivities to SKF89976A, which together with the different voltage-dependent fluorescence changes in Na^+ and Li^+ buffer, suggests that *the cation-dependent conformational changes of GAT-1 are global and not only due to a minor alteration of the microenvironment around Cys^{74}.* This finding is in line with a previous study on zinc-site engineering into GAT-1, in which the Li^+-induced current and the GABA transport were inhibited differentially and oppositely by the addition of Zn^{2+} to the test solution, indicating that the conformations and/or the voltage-dependent conformational changes of GAT-1 are indeed depending on the presence of Na^+ or Li^+ (6).

What Causes the Voltage-dependent Fluorescence Intensity Changes?—The application of the voltage clamp fluorometry method to investigate protein conformational changes has been applied to several cotransporters, including SGLT-1(13, 18), GAT-1 (43), serotonin transporter (44), EAAT3 (45), and the Na/P_i transporter (NaP_i) (46, 47). Changes in fluorescence intensity are due to changes in the emission spectrum, quantum yield, or absorption spectrum as a result of alterations in the local physical and electronic environment of the fluorophore (48). Although in principle, it is possible that changes in the dielectric environment of the fluorophore *per se* (in the absence of protein movement) may contribute to fluorescence changes, our modeling of the changes of the local physical environment of the fluorophore attached to Cys^{74} suggests that the fluorescence changes are associated with the motion of the transporter (see below).

To obtain direct evidence for the conformational differences between a Na^+-bound and Li^+-bound GAT-1, high resolution crystal structures of GAT-1 obtained in Na^+ or Li^+ would be needed. However, a homology model of GAT-1 with TMR6M covalently bound to Cys^{74} (Fig. 1, *A* and *B*) and the speculative conformational arrangement of the outward and inward facing states that has been proposed with the two crystal structures of $LeuT_{Aa}$ and a model thereof (15, 26, 49) provide some clues about how and where the voltage-dependent fluorescence changes may arise. In general, a more hydrophobic and less polar environment of the fluorophore increases the quantum yield of the TMR6M fluorescence (50). In the homology model, GAT-1 is in an occluded state with Na^+, Cl^-, and GABA bound. In this conformation, TMR6M bound to Cys^{74} is situated in a hydrophobic pocket between extracellular loop three (EL3) connecting TM5 and TM6 and extracellular loop four (EL4) connecting TM7 and TM8 suggesting that the fluorophore is in close contact with the protein, emphasized by possible formations of hydrogen bonding between TMR6M and Thr^{273} and Lys^{350} (Fig. 1*B*). The voltage-dependent changes in fluorescence intensity that we observe may be explained by a closed arrangement of EL3/EL4 and the outer part of TM1 in the inward facing conformation (NaCl buffer, C_6) and an open arrangement of EL3/EL4 and the outer part of TM1 in the open Li-bound state (LiCl buffer, C_1LiO). See Fig. 6 in Ref. 15 for details on structural organization. There are several hydrophobic amino acids in EL3 (*i.e.* Gly^{267}, Phe^{270}, and Tyr^{271}), EL4 (*i.e.* Phe^{336}, Ile^{341}, and Phe^{344}), and TM1 (*i.e.* Gly^{79} and Gly^{80}) that may contribute to a local hydrophobic environment of the fluorophore. It has previously been suggested that EL4 of GAT-1 moves as the protein undergoes conformational changes (51, 52), which is in good agreement with our fluorescence data in combination with the homology model.

Comparison to Other Studies—It was previously shown that labeling of rat GAT-1 with small membrane-impermeable MTS reagents blocked the GABA-coupled currents as well as the transient currents (23), whereas labeling with the fluorophore tetramethylrhodamine 5-maleimide has been shown not to alter GAT-1 function significantly (43). In the study by Li *et al.* (43), the use of simultaneous voltage clamp and fluorescence experiments was applied to rat GAT-1 labeled with tetramethylrhodamine 5-maleimide. These experiments gave rise to voltage-dependent fluorescent changes of a slightly smaller magnitude (0.8 *versus* 1.1%), lower resolution, and different kinetics than those observed in the present study with TMR6M. The discrepancies between the two studies are most likely due to the difference in the structure of the two isomers of the fluorophore.

Conclusion—We have in the present study found evidence supporting our hypothesis that Li^+ occupies the first cation-binding site of GAT-1 and "stalls" the protein in a conformation from which the Li^+-induced leak current appears at potentials more negative than −50 mV due to a voltage-dependent conformational change that is specific to the Li^+-bound transporter (both with regard to the voltage dependence and with regard to the time constants of the process). The voltage-dependent fluorescent changes as well as the Li^+-induced leak current show saturation at the most hyperpolarized potentials, which points to the leak current being a channel mode of action (a transfer from one conformation to another as opposed to a continuous cycling). The increase in $IC_{50(SKF89976A)}$ by replacement of Na^+ with Li^+ in the buffer supports the notion that the conformation and/or the conformational changes associated with Li^+ (C_1Li and/or $C_1Li \leftrightarrow C_1LiO$ in the model) is distinct from the conformation and/or the conformational changes with two Na^+ bound ($C_6 \leftrightarrow C_0 \leftrightarrow C_1Na \leftrightarrow C_2Na_2$ in the model). The Na^+-dependent transient currents are directly associated with the conformational changes taking place upon the binding and unbinding of sodium ions as shown by the correlation of the voltage dependence as well as the time constants for the global conformational changes underlying the transient currents and the local conformational changes taking place at Cys^{74}.

Taken together, these findings show that the time course and voltage dependence of the changes of the local environment in the external surface of TM1 agree with the time course and the voltage dependence of the global conformational changes underlying the transient currents as well as the leak current. We predict that voltage clamp fluorometry, combined with homology modeling, will be a powerful technique in the aim of deducing the structural dynamics taking place in cotransport proteins.

Acknowledgment—We thank Tove Soland for preparation of X. laevis oocytes.

REFERENCES

1. Borden, L. A. (1996) *Neurochem. Int.* **29,** 335–356
2. Radian, R., and Kanner, B. I. (1983) *Biochemistry* **22,** 1236–1241
3. Keynan, S., and Kanner, B. I. (1988) *Biochemistry* **27,** 12–17
4. Mager, S., Kleinberger-Doron, N., Keshet, G. I., Davidson, N., Kanner, B. I., and Lester, H. A. (1996) *J. Neurosci.* **16,** 5405–5414
5. Bismuth, Y., Kavanaugh, M. P., and Kanner, B. I. (1997) *J. Biol. Chem.* **272,** 16096–16102
6. MacAulay, N., Bendahan, A., Loland, C. J., Zeuthen, T., Kanner, B. I., and Gether, U. (2001) *J. Biol. Chem.* **276,** 40476–40485
7. Mager, S., Naeve, J., Quick, M., Labarca, C., Davidson, N., and Lester, H. A. (1993) *Neuron* **10,** 177–188
8. MacAulay, N., Zeuthen, T., and Gether, U. (2002) *J. Physiol.* **544,** 447–458
9. Mager, S., Min, C., Henry, D. J., Chavkin, C., Hoffman, B. J., Davidson, N., and Lester, H. A. (1994) *Neuron* **12,** 845–859
10. Sonders, M. S., Zhu, S. J., Zahniser, N. R., Kavanaugh, M. P., and Amara, S. G. (1997) *J. Neurosci.* **17,** 960–974
11. Hirayama, B. A., Loo, D. D., and Wright, E. M. (1997) *J. Biol. Chem.* **272,** 2110–2115
12. Zhou, Y., Zomot, E., and Kanner, B. I. (2006) *J. Biol. Chem.* **281,** 22092–22099
13. Loo, D. D., Hirayama, B. A., Gallardo, E. M., Lam, J. T., Turk, E., and Wright, E. M. (1998) *Proc. Natl. Acad. Sci. U. S. A.* **95,** 7789–7794
14. Borden, L. A., Murali Dhar, T. G., Smith, K. E., Weinshank, R. L., Branchek, T. A., and Gluchowski, C. (1994) *Eur. J. Pharmacol.* **269,** 219–224
15. Yamashita, A., Singh, S. K., Kawate, T., Jin, Y., and Gouaux, E. (2005) *Nature* **437,** 215–223
16. Loo, D. D., Hazama, A., Supplisson, S., Turk, E., and Wright, E. M. (1993) *Proc. Natl. Acad. Sci. U. S. A.* **90,** 5767–5771
17. Zhang, H., and Karlin, A. (1997) *Biochemistry* **36,** 15856–15864
18. Meinild, A. K., Hirayama, B. A., Wright, E. M., and Loo, D. D. F. (2002) *Biochemistry* **41,** 1250–1258
19. Beuming, T., Shi, L., Javitch, J. A., and Weinstein, H. (2006) *Mol. Pharmacol.* **70,** 1630–1642
20. Sali, A., and Blundell, T. L. (1993) *J. Mol. Biol.* **234,** 779–815
21. Schrödinger, L. (2008) *Schrödinger Suite 2008 Induced Fit Docking Protocol,* Schrödinger LLC, New York
22. DeLano, W. L. (2002) *The PyMOL Molecular Graphics System*, DeLano Scientific, Palo Alto, CA
23. Yu, N., Cao, Y., Mager, S., and Lester, H. A. (1998) *FEBS Lett.* **426,** 174–178
24. Golovanevsky, V., and Kanner, B. I. (1999) *J. Biol. Chem.* **274,** 23020–23026
25. Hazama, A., Loo, D. D., and Wright, E. M. (1997) *J. Membr. Biol.* **155,** 175–186
26. Forrest, L. R., Zhang, Y. W., Jacobs, M. T., Gesmonde, J., Xie, L., Honig, B. H., and Rudnick, G. (2008) *Proc. Natl. Acad. Sci. U. S. A.* **105,** 10338–10343
27. Bennett, E. R., Su, H., and Kanner, B. I. (2000) *J. Biol. Chem.* **275,** 34106–34113
28. Kanner, B. I. (2003) *J. Biol. Chem.* **278,** 3705–3712
29. Melamed, N., and Kanner, B. I. (2004) *Mol. Pharmacol.* **65,** 1452–1461
30. Zhou, Y., Bennett, E. R., and Kanner, B. I. (2004) *J. Biol. Chem.* **279,** 13800–13808
31. Zomot, E., Zhou, Y., and Kanner, B. I. (2005) *J. Biol. Chem.* **280,** 25512–25516
32. Zhou, Y., and Kanner, B. I. (2005) *J. Biol. Chem.* **280,** 20316–20324
33. Umbach, J. A., Coady, M. J., and Wright, E. M. (1990) *Biophys. J.* **57,** 1217–1224
34. Galli, A., DeFelice, L. J., Duke, B. J., Moore, K. R., and Blakely, R. D. (1995) *J. Exp. Biol.* **198,** 2197–2212
35. Chen, J. G., Liu-Chen, S., and Rudnick, G. (1997) *Biochemistry* **36,** 1479–1486
36. Ni, Y. G., Chen, J. G., Androutsellis-Theotokis, A., Huang, C. J., Moczydlowski, E., and Rudnick, G. (2001) *J. Biol. Chem.* **276,** 30942–30947
37. López-Corcuera, B., Núñez, E., Martínez-Maza, R., Geerlings, A., and Aragón, C. (2001) *J. Biol. Chem.* **276,** 43463–43470
38. Lin, F., Lester, H. A., and Mager, S. (1996) *Biophys. J.* **71,** 3126–3135
39. Wadiche, J. I., Arriza, J. L., Amara, S. G., and Kavanaugh, M. P. (1995) *Neuron* **14,** 1019–1027
40. Bicho, A., and Grewer, C. (2005) *Biophys. J.* **89,** 211–231
41. Liu, Y., Eckstein-Ludwig, U., Fei, J., and Schwarz, W. (1998) *Biochim. Biophys. Acta* **1415,** 246–254
42. Hilgemann, D. W., and Lu, C. C. (1999) *J. Gen. Physiol.* **114,** 459–475
43. Li, M., Farley, R. A., and Lester, H. A. (2000) *J. Gen. Physiol* **115,** 491–508
44. Li, M., Farley, R. A., and Lester, H. A. (2002) *FEBS Lett.* **513,** 247–252
45. Larsson, H. P., Tzingounis, A. V., Koch, H. P., and Kavanaugh, M. P. (2004) *Proc. Natl. Acad. Sci. U. S. A.* **101,** 3951–3956
46. Virkki, L. V., Murer, H., and Forster, I. C. (2006) *J. Gen. Physiol.* **127,** 539–555
47. Virkki, L. V., Murer, H., and Forster, I. C. (2006) *J. Biol. Chem.* **281,** 28837–28849
48. Bezanilla, F. (2000) *Physiol. Rev.* **80,** 555–592
49. Singh, S. K., Yamashita, A., and Gouaux, E. (2007) *Nature* **448,** 952–956
50. Mannuzzu, L. M., and Isacoff, E. Y. (2000) *J. Gen. Physiol.* **115,** 257–268
51. MacAulay, N., Meinild, A. K., Zeuthen, T., and Gether, U. (2003) *J. Biol. Chem.* **278,** 28771–28777
52. Zomot, E., and Kanner, B. I. (2003) *J. Biol. Chem.* **278,** 42950–42958